
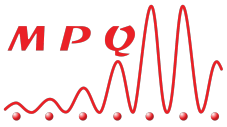

Developing Pulsed Laser Ablation in Liquid for the Synthesis of Gold Colloids

Francesco Monni

Supervisor:
Damien Alloyeau

Nanotechnologies for ICTs – Double Degree Programme
M2 – Quantum Devices (NanoQuad)

Paris
June 2025

Contents

Abstract

This report presents the design, development, and optimization of a setup for the synthesis of gold nanoparticles (Au NPs) via Pulsed Laser Ablation in Liquid, using a KrF excimer laser (of 248 nm wavelength). The setup was entirely assembled during the internship, with particular attention to beam alignment, target positioning, and system reproducibility. Using pure water as the initial liquid medium, the work investigates the role of laser parameters such as fluence and irradiation time, as well as the influence of ligands on the morphology and stability of the resulting colloids. After observing significant aggregation in water, trisodium citrate dihydrate was introduced to improve colloidal stability.A detailed analysis of concentration effects revealed that a TCD concentration between 10^{-4} and 10^{-3} M not only minimized aggregation but also influenced the overall synthesis dynamics. UV-Vis spectroscopy and TEM were employed to characterize the optical and structural features of the nanoparticles. This work provides a reproducible framework to produce Au NPs with tunable properties and offers insights into the interplay between ablation and irradiation processes.

1 Introduction

Gold nanoparticles (Au NPs) have emerged as one of the most extensively studied nanomaterials, due to their unique optical, electronic, and chemical properties. These characteristics, especially their localized surface plasmon resonance (LSPR), are highly sensitive to particle size and shape, making Au NPs suitable for applications in biosensing, catalysis, photothermal therapy, and drug delivery. As a result, significant efforts have been devoted to the development of reliable and controllable synthesis strategies. Traditional chemical methods, such as the Turkevich protocol, are widely used and provide effective size control. However, they typically involve stabilizing agents that can alter surface chemistry and interfere with the functionality of the particles, especially in applications that require clean surfaces. For this reason, physical synthesis approaches have gained growing attention. Pulsed Laser Ablation in Liquid (PLAL) is a promising technique in this context, as it allows the production of high yield colloidal nanoparticles without the use of surfactants or chemical precursors. The process involves focusing high-energy laser pulses onto a metal target submerged in a liquid medium, resulting in plasma formation and nanoparticle nucleation.

This work focuses on the development and optimization of a PLAL setup based on a KrF excimer laser, fully assembled during the internship. The effect of key synthesis parameters such as laser fluence, irradiation time, and the chemical composition of the liquid was systematically studied. In addition to the physical synthesis route, a set of gold nanoparticles was also synthesized using a citrate-based chemical reduction method, in order to highlight the differences in morphology, stability, and optical properties between the two approaches. Characterization of the nanoparticles was performed using UV–Vis spectroscopy and Transmission Electron Microscopy (TEM), allowing a comprehensive assessment of their size distribution, shape, and colloidal behavior. The results provide practical insight into how synthesis conditions affect nanoparticle features and contribute to a deeper understanding of the physical and chemical mechanisms involved in gold colloid formation.

2 Presentation of Laboratory and Team

The Materials and Quantum Phenomena Laboratory (MPQ) is a Joint Research Unit (UMR 7162) affiliated with the French National Center for Scientific Research (CNRS) and Université Paris Cité. The lab focuses on the study of quantum materials and the development of novel quantum devices, bringing together theoretical and experimental expertise in condensed matter physics, transport, and optics. Its research activities are supported by advanced technological platforms, including clean-room nanofabrication facilities, high-resolution spectroscopy, and state-of-the-art electron microscopy.

This internship was carried out within the MEANS group (Advanced Electron Microscopy and Nano-Structures), under the supervision of Professor Damien Alloyeau. The group develops both synthesis strategies and in situ electron microscopy techniques to investigate the structure, dynamics, and transformation of nanomaterials at the atomic scale. Its research is centered on the formation and evolution of nanoalloys, nucleation and growth in liquid environments, and the life-cycle of nanostructures in biological or environmental media. A particular expertise of this group lies in the use of liquid- and gas-cell transmission electron microscopy, including the JEOL aberration-corrected SUPER TEM, to study nanomaterials in realistic operating conditions. It is worth noting that the team also conducts research on Pulsed Laser Deposition in vacuum. However, this work marks the first time the ablation process was carried out in a liquid environment within the group, with the view to develop a high yield synthesis method of metallic nanoparticles and nanoalloys.

3 State of the Art

3.1 Nanoparticle Synthesis and Colloidal Stability

The synthesis of gold nanoparticles (Au NPs) has been extensively explored due to their tunable optical and electronic properties, which arise from their size-dependent localized surface plasmon resonance (LSPR). These features enable applications in biomedicine, catalysis, and sensing. Among the most established synthesis routes, chemical reduction methods offer a simple and scalable strategy for producing colloidal Au NPs with controlled dimensions. In these processes, reducing agents not only promote the formation of nanoparticles by reducing gold salts to metallic Au, but also act as stabilizers, preventing uncontrolled growth and aggregation. This dual function helps maintain colloidal stability and uniformity across batches [9, 14].

The chemical environment plays a fundamental role in stabilization. Citrate ions, for instance, adsorb onto the particle surface and generate a negative surface charge, creating an electrostatic barrier that prevents van der Waals–driven aggregation. According to DLVO theory, colloidal stability arises from the balance between attractive van der Waals forces and repulsive electrostatic interactions due to the electrical double layer surrounding each particle. When the repulsive potential dominates, it creates an energy barrier that prevents particle coalescence [9]. This mechanism makes chemical synthesis particularly effective in maintaining stable dispersions over time.

However, purely chemical routes often leave residual ligands on the nanoparticle surface, which can interfere with catalytic performance or hinder subsequent functionalization. For applications requiring ultra-clean surfaces, Pulsed Laser Ablation in Liquid (PLAL) offers a more suitable alternative. In this physical method, a metal target submerged in a liquid medium is irradiated with pulsed laser energy, generating a high-temperature plasma and a cavitation bubble that leads to nanoparticle nucleation and ejection into the surrounding fluid [5, 24]. Ideally, PLAL requires no chemical precursors or surfactants, enabling the production of surfactant-free, high-purity Au NPs. However, nanoparticles synthesized in pure solvents like deionized water are often unstable due to the absence of strong capping agents. Aggregation is frequently reported and has been attributed to the high surface energy of naked metallic particles [1, 14].

To address this limitation, ligands such as trisodium citrate dihydrate (TCD) can be introduced into the liquid medium. While PLAL still allows for clean synthesis, the presence of low concentrations of citrate provides electrostatic stabilization without heavily modifying the particle surface. The use of TCD creates a controlled environment where the aggregation rate is suppressed, the optical properties are preserved, and the nanoparticles remain monodispersed. As shown in multiple studies, optimal TCD concentrations fall in the range of 10^{-4} to 10^{-3} M, balancing nucleation dynamics and colloidal stability [5, 23]. However, while citrate is widely used as a stabilizing ligand, many studies do not specify its exact concentration or systematically explore its influence.

3.2 Objectives of the Work

The main goal of this internship was to understand how individual synthesis parameters influence the formation, morphology, and stability of gold nanoparticles produced by Pulsed Laser Ablation in Liquid (PLAL). To do so, a dedicated experimental setup was designed and assembled to enable controlled experimental conditions, allowing a systematic investigation of the key physical and chemical variables involved. The project focused on solving four main challenges:

- **Reproducibility:** Slight misalignments in the experimental setup or fluctuations in laser fluence can drastically alter the outcome. Ensuring reproducibility across multiple experiments was therefore a critical objective of this work.
- **Parameter isolation:** In many studies, synthesis parameters are varied simultaneously, making it difficult to attribute observed effects to a specific cause. A major objective here was to decouple the influence of fluence, repetition rate, irradiation time, ablation time, and ligand concentration to gain clearer insights into their individual roles in influencing the final nanoparticle properties.
- **Synthesis optimization:** Optimizing the synthesis process is essential in order to obtain the desired nanoparticle features, that may vary depending on the specific application. The challenge was to define and reach target outcomes by tuning the appropriate synthesis parameters, requiring a clear connection between processing conditions and final product features.
- **Ligand concentration:** Beyond simply preventing aggregation, ligand concentration directly impacts nanoparticle formation, influencing size distribution, morphology, and optical response. A key challenge was to understand how small variations in stabilizer concentration could be strategically used to modify the synthesis outcome.
- **Ablation and Irradiation:** In PLAL synthesis, target ablation and solution irradiation occur simultaneously, making it difficult to isolate their respective contributions. A key objective of this work was to decouple these effects in order to clarify their individual impact on nanoparticle formation and evolution.

By addressing these challenges, this work establishes a robust and reproducible framework for PLAL synthesis and provides practical insights into tuning gold nanoparticle properties through systematic control of synthesis parameters.

4 Experimental setup

A central aspect of this internship was the complete design and assembly of the experimental setup for the ablation experiments. The system was constructed entirely from scratch using available laboratory components and integrated onto a pre-existing beamline. Particular attention was paid to the alignment of optical elements, the mechanical stability of the sample holder, and the reproducibility of operating conditions.

All ablation and irradiation experiments discussed in this report were carried out independently by me. I was also personally responsible for the investigation of the resulting nanoparticles using transmission electron microscopy (TEM) and UV–Vis spectroscopy, as well as for the subsequent data analysis and interpretation.

4.1 Laser Ablation and Irradiation Configuration

In this report, the following terms will be consistently used:

- **Ablation**: the process in which material is removed from the gold target due to high-energy laser pulses and dispersed into the surrounding solution (Figure 1). A 100 mL beaker was used for these experiments.

- **Irradiation**: additional exposure of an already synthesized colloidal solution to the laser beam. The irradiation setup closely mirrors the ablation configuration, except that a smaller 5 mL beaker was employed here instead (Figure 2).

It is important to note that during any ablation experiment, the laser beam also interacts with the surrounding liquid, meaning that irradiation inherently occurs as a side effect. However, in the dedicated irradiation experiments carried out in this work, the gold target was removed, allowing for a pure irradiation process to take place. A graphical representation of the experimental setups for ablation and irradiation experiments is shown in Figures 1 and 2 respectively:

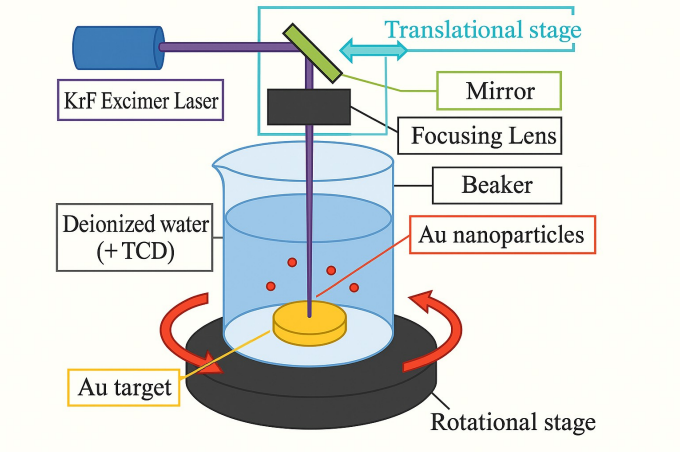

Figure 1: Schematic representation of the experimental setup for Pulsed Laser Ablation in Liquid (PLAL). A KrF excimer laser irradiates a gold target placed on a Teflon disk at the bottom of a rotating beaker containing deionized water and TCD. Rotation of the target and translation of the mirror ensures uniform target ablation and liquid stirring. Adapted from Alluhaybi et al. [5].

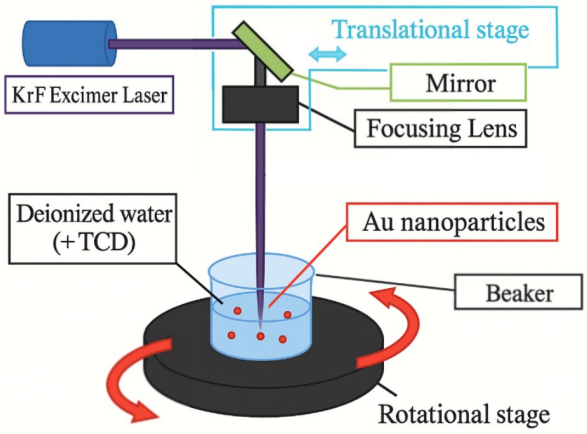

Figure 2: Schematic representation of the experimental setup used for laser irradiation experiments. Rotation of the stage ensures liquid stirring. Adapted from Alluhaybi et al. [5].

All experiments were conducted using a KrF excimer laser (wavelength $\lambda = 248$ nm, 25 nanoseconds pulse duration). The gold target, shaped like a coin, was thoroughly cleaned with ethanol and mechanically polished using abrasive paper before each experiment to ensure surface uniformity. It was positioned at the center of a custom-made Teflon disk placed at the bottom of the beaker, ensuring both mechanical stability and precise alignment. The laser beam was directed vertically onto the target surface by a UV mirror mounted at a 45° angle. A lens with a 30 cm focal length, positioned horizontally, focused the beam onto a spot of approximately 0.03 cm^2. Both mirror and lens were fixed on a motorized translation stage, enabling continuous horizontal scanning over the target surface. Coupled with a rotating platform beneath the beaker, this arrangement guaranteed uniform ablation, avoiding crater formation.

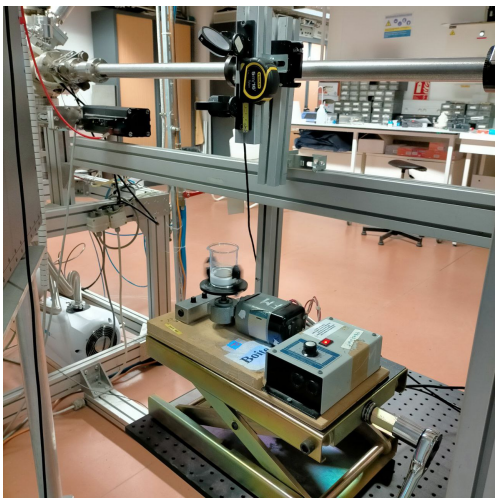

(a) Complete experimental setup for PLAL and irradiation experiments.

(b) KrF excimer laser (248 nm), model COMPex PRO 102 F by Coherent GmbH, used as the light source for all experiments.

Figure 3: Experimental apparatus used for laser ablation and irradiation experiments. (a) Entire experimental setup showing optical elements and sample stage. (b) KrF excimer laser.

Standard 100 mL borosilicate glass beakers were used for ablation experiments, filled up to the 40 mL mark. However, due to the space occupied by the Teflon disk, the effective liquid volume was approximately 13 mL. All experiments were performed with the beaker left open to the atmosphere. The following parameters were systematically varied during the experiments:

- Laser pulse energy: 100–300 mJ
- Laser fluence: 0.31–3.07 J/cm^2
- Repetition rate: 1–10 Hz
- Irradiation time: 5–60 minutes
- TCD concentration: 0 M (pure water), 10^{-5} M, 10^{-4} M, 10^{-3} M, 10^{-2} M, 10^{-1} M
- Beaker size: 100 mL beaker for ablation; 5 mL beaker for irradiation

This setup was designed to ensure high reproducibility and flexibility across a wide range of experimental conditions. By precisely controlling each parameter and ensuring uniform laser-target interaction, it was possible to systematically investigate how individual synthesis variables affect nanoparticle formation, morphology, and stability. The following sections present a detailed analysis of these effects.

Transmission Electron Microscopy (TEM)

To investigate nanoparticle morphology, transmission electron microscopy (TEM) analysis was carried out using a JEOL JEM-2100 microscope (shown in Figure 4). A few microliters of each colloidal solution were drop-cast onto carbon-coated copper lacey TEM grids and allowed to dry at ambient conditions. The samples were not subjected to centrifugation or filtration prior to imaging in order to preserve the native size distribution. TEM analysis was used to evaluate average size, minimum and maximum dimensions, and aspect ratio of the nanoparticles. DigitalMicrograph software was employed to manually analyze the particle outlines and extract morphological parameters from multiple images per sample. The measurements were used to generate the statistical plots shown in the Results section.

Figure 4: JEOL JEM-2100 transmission electron microscope used for nanoparticle imaging and morphological analysis. The instrument was operated to acquire TEM images for evaluating size, shape, and aspect ratio of the synthesized nanoparticles.

UV–Vis Absorbance Spectroscopy

Optical characterization of the colloidal solutions was performed using a JASCO V-630 UV–Vis spectrophotometer (Figure 5). Spectra were recorded in the range of 350–800 nm with a resolution of 1 nm. Quartz cuvettes with 1 cm path length were used for all measurements. After the absorbace data was collected, background correction was applied using deionized water as a blank.

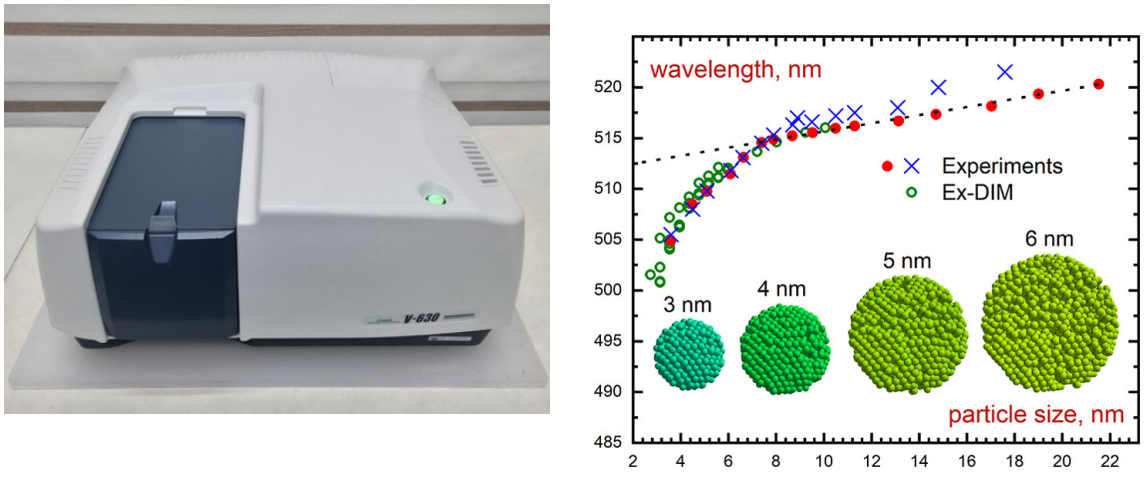

(a) (b)

Figure 5: (a) JASCO V-630 spectrophotometer used for UV–Vis absorbance measurements. (b) Peak position in the localized surface plasmon resonance spectrum as a function of particle size (adapted from [19]).

The evolution of the surface plasmon resonance (SPR) peak was tracked to monitor changes in nanoparticle size, shape, and concentration as a function of irradiation time and synthesis conditions. Key observations included blue-shift or red-shift behavior, peak broadening, and absorbance intensity, all of which were used to infer the aggregation state and optical density of the nanoparticle dispersions.

5 Results and discussion

This section presents and discusses the results obtained from a systematic study on the synthesis of gold nanoparticles via Pulsed Laser Ablation in Liquid. Various key parameters were carefully explored and optimized, including laser fluence, pulse energy, repetition rate, irradiation time, and ligand concentration. Initially, experiments conducted in pure water revealed significant nanoparticle aggregation, prompting the introduction of trisodium citrate dihydrate as a stabilizing agent. Detailed analyses of the synthesized colloids were performed using Transmission Electron Microscopy (TEM) and UV-Vis spectroscopy to evaluate nanoparticle size, morphology, and optical properties. The following subsections illustrate the effects of each parameter variation, providing insights into achieving stable and reproducible Au nanoparticle colloids.

5.1 PLA in pure H_2O

The initial synthesis experiments were carried out using pure deionized water as the ablation medium. This choice was guided by several studies that reported successful laser ablation in liquid using water alone, without the need for stabilizing ligands. For instance, Alluhaybi et al. [5] demonstrated the formation of gold nanoparticles with distinct optical features in water, highlighting the simplicity of the approach. Similarly, Schmidl et al. [16] employed pulsed UV laser treatment in aqueous environments to fabricate spherical gold particles via self-assembly. These precedents suggested that under controlled parameters, pure water could support colloidal nanoparticle synthesis without requiring chemical additives. In our case, we adopted a comparable strategy and irradiated a gold target in deionized water using a KrF excimer laser. Our goal was to replicate and evaluate the extent to which stable and well-dispersed nanoparticles could be synthesized in the absence of any surfactants, reducing agents, or other stabilizing molecules.

However, despite the theoretical appeal, our observations revealed a different outcome. TEM analysis showed pronounced aggregation of the nanoparticles, with large, irregular clusters forming throughout the sample. This aggregation occurred regardless of the laser fluence or repetition rate applied within our typical parameter space. Unlike the relatively monodisperse and stable systems described in [5] and [16], the particles in our case appeared to coalesce rapidly after ablation, indicating insufficient colloidal stabilization. This outcome aligns with broader findings in the literature, which emphasize that while water can support initial nucleation and growth, the lack of electrostatic barriers makes the particles highly prone to agglomeration [21]. Therefore, although water is an attractive medium for PLAL due to its simplicity and low toxicity, our results underscore its limitations for generating stable colloids without post-synthesis stabilization. The presence of aggregation can be clearly seen in Figure 6:

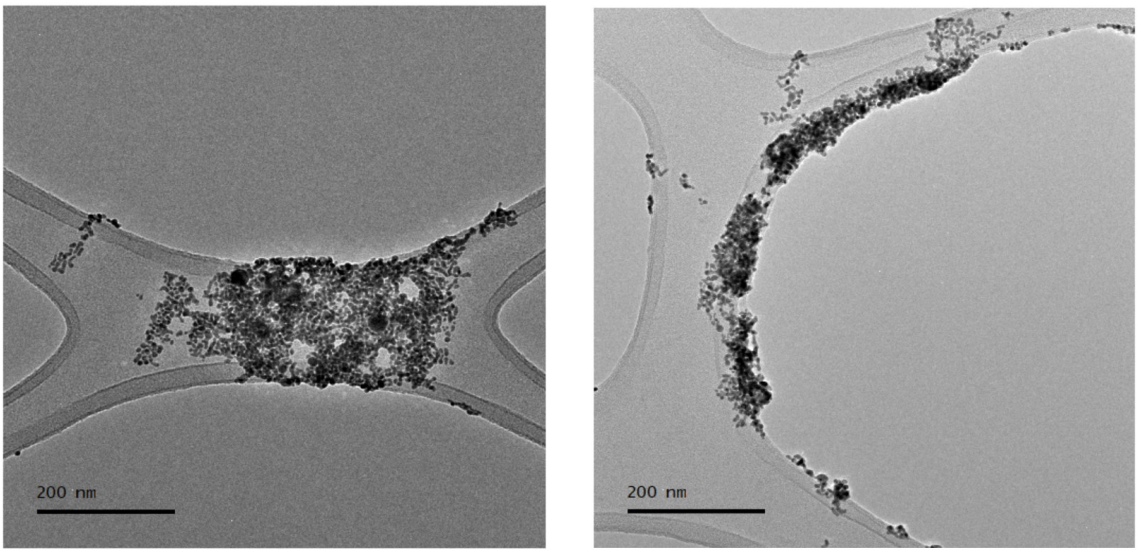

Figure 6: TEM images of Gold nanoparticles synthesized in a pure water environment, under a fluence of 3.00 J/cm^2 and repetition rate 5 Hz for 15 minutes.

Ablation in pure H_2O: Effect of Fluence

Despite aggregation, the size of individual nanoparticles could still be measured from the TEM images. To evaluate the effect of laser fluence on nanoparticle morphology, a set of ablation experiments in pure water was carried out at a fixed irradiation time of 15 minutes. In each of these, the fluence was varied between 2.5 and 5.0 J/cm^2, while keeping all the other parameters constant. Nanoparticles were successfully synthesized across this range, as all fluence values exceeded the typical ablation threshold reported in literature, which lies between 1.2 and 1.6 J/cm^2 for gold targets in water [5, 16]. Analysis of the resulting samples revealed only a limited influence of fluence on size-related metrics. Average, minimum, and maximum diameters showed only minor variations, with largely overlapping error bars, as seen in Figure 7. A slight increase in average size is observed at 3.3 J/cm^2, but this change is not statistically significant. The same holds true for the aspect ratio, which remains nearly constant across the tested fluence range.

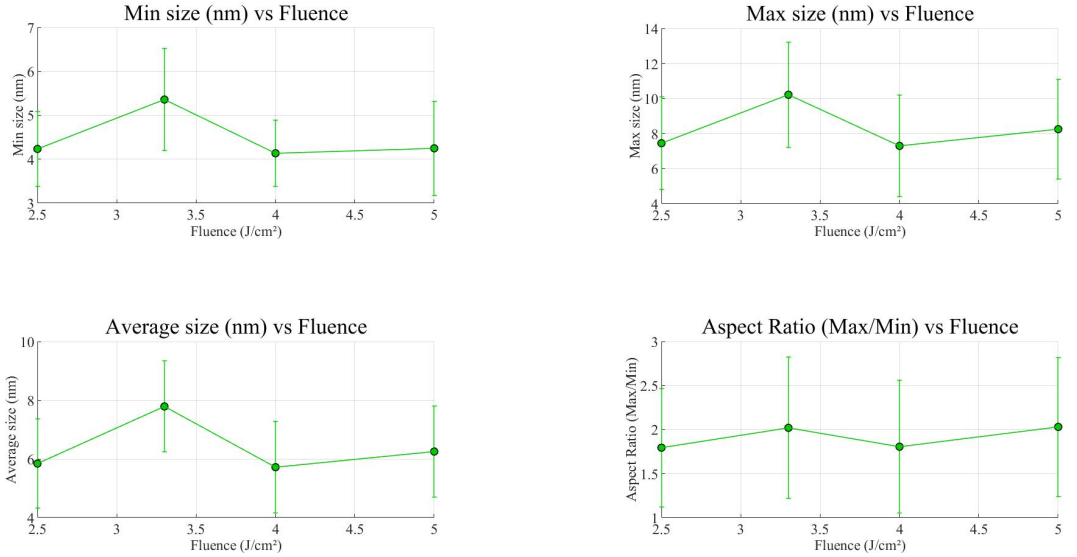

Figure 7: Morphological evolution of nanoparticles under 15 min ablation at varying fluence.

The fluence dependence observed in this study aligns with previous reports [8, 21], which show that once the energy delivered to the system exceeds the ablation threshold, further increases have only a limited effect on nanoparticle size and shape. This behavior is often attributed to plasma shielding, which can counterbalance the increased energy input. In a pure water environment, these effects are more directly reflected in the final nanoparticle population, as no stabilizing agent is present to mitigate aggregation or shape fluctuations. Overall, fluence within this range does not appear to be a dominant parameter in controlling morphology. Other factors, such as irradiation time or the presence of stabilizing ligands, are likely to play a more significant role and will be explored in the following sections.

Ablation in Pure H_2O: Effect of Repetition Rate

The influence of repetition rate on nanoparticle morphology was studied by varying it between 1, 5, and 10 Hz, while keeping fluence and irradiation time constant at 3.3 J/cm^2 and 15 minutes, respectively. As shown in Figure 8, the effect of this parameter is relatively modest. A small increase in average and maximum size is observed at 5 Hz, followed by a slight decrease at 10 Hz. The aspect ratio also follows a similar trend, with a maximum around the intermediate value.

These results suggest that repetition rate does play a role in influencing particle growth dynamics through mechanisms such as cumulative heating or increased local particle density near the target surface. Similar conclusions have been reported in earlier studies [5, 21], where particle size and shape distributions were primarily driven by laser energy density and solution composition, with repetition rate showing only secondary effects. As shown in the TEM images in Figure 8, strong

aggregation was observed across all samples, making it difficult to extract clear morphological differences at the individual particle level. This highlights the limitations of working in pure water without stabilizing ligands and reinforces the need for surface passivation strategies to better control nanoparticle dispersion.

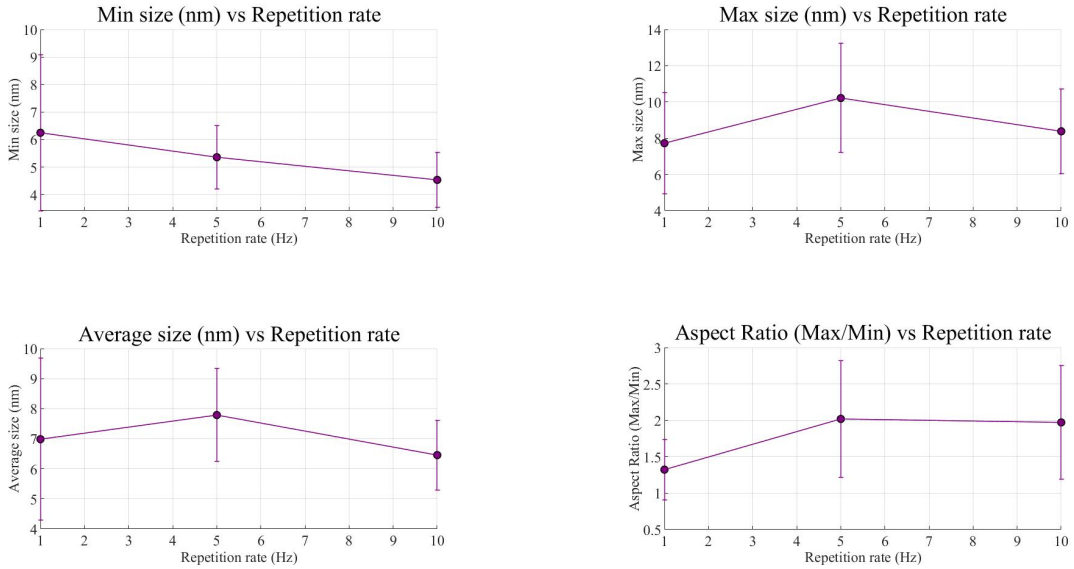

Figure 8: Effect of repetition rate on nanoparticle morphology after a 15 minutes ablation at 3.33 J/cm^2.

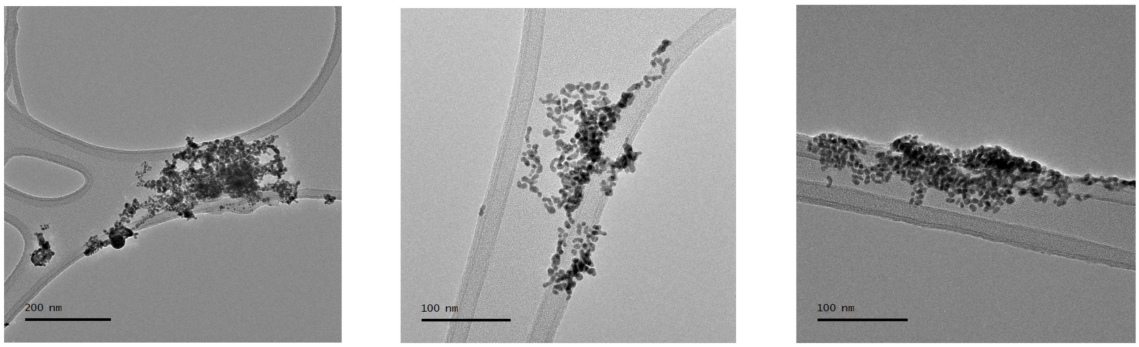

(a) 1 Hz (b) 5 Hz (c) 10 Hz

Figure 9: TEM images of nanoparticles obtained after 15 minutes of ablation at 3.3 J/cm^2, under different repetition rates.

5.2 Introducing Ligands: the Effect of Concentration

To mitigate nanoparticle aggregation during laser ablation, stabilizing ligands were introduced into the liquid medium. In pure water, aggregation becomes increasingly problematic with longer ablation times, compromising both the optical response of the colloid and the reliability of TEM characterization. The addition of ligands helps maintain particle dispersion over time, improving stability, reproducibility, and overall quality of the synthesized nanoparticles. Three candidate ligands were initially considered: 1-butanethiol, sodium dodecyl sulfate, and trisodium citrate dihydrate (TCD). TCD was selected for further testing because of its ease of handling, chemical stability, and low toxicity, making it safer and more practical for routine laboratory use.

A range of concentrations was explored to identify an optimal window that balances particle formation with colloidal stability. The observed behavior can be categorized as follows:

- **Below 10^{-4} M:** Stabilization was insufficient to prevent aggregation. TEM images revealed strong clustering and poor colloidal stability.
- **Between 10^{-4} M and 10^{-3} M:** Well-dispersed particles were obtained with significantly reduced aggregation. This range appears to offer the best trade-off between nucleation efficiency and colloidal stability.
- **Above 10^{-3} M:** No visible color change was observed, and TEM analysis confirmed the absence of nanoparticles. This suggests that an excess of citrate may inhibit nucleation or growth by over-passivating the gold surface.

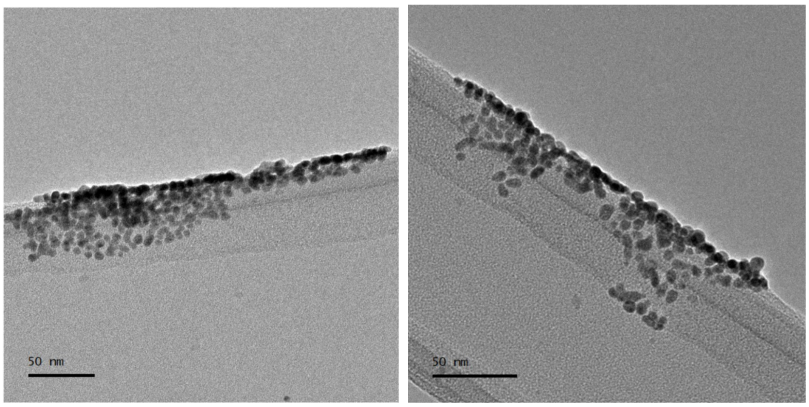

(a) Pure H_2O (b) Pure H_2O

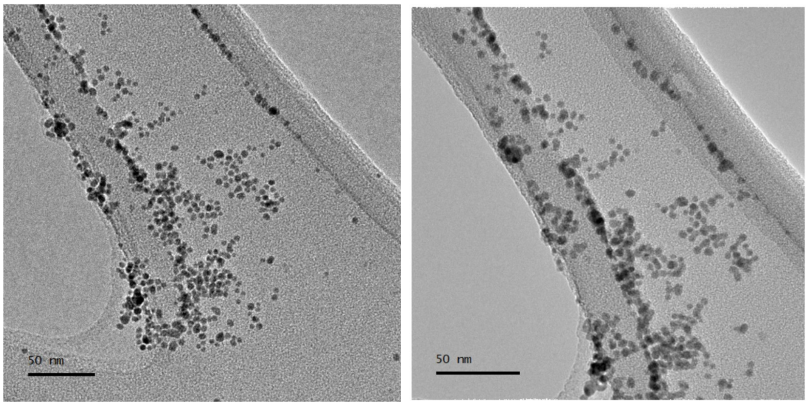

(c) TCD 10^{-4} M (d) TCD 10^{-4} M

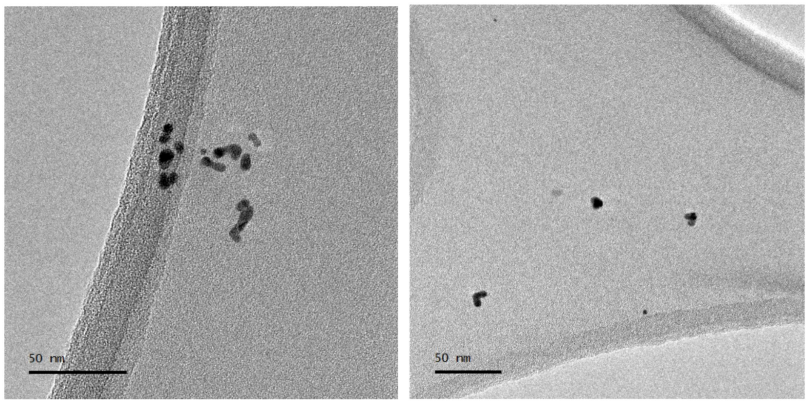

(e) TCD 10^{-3} M (f) TCD 10^{-3} M

Figure 10: TEM images of nanoparticles synthesized via laser ablation in liquids with varying TCD concentrations. Significant aggregation is visible in pure water (a, b), while dispersion improves markedly with the addition of TCD at 10^{-4} M (c, d) and 10^{-3} M (e, f). All samples were produced under identical conditions: fluence of 3.07 J/cm^2, repetition rate of 5 Hz, and an ablation time of 30 minutes.

This trend is clearly evident in the TEM images presented in Figure 10, which illustrate the impact of TCD on nanoparticle dispersion. In the absence of stabilizers (pure water), extensive aggregation occurs, making individual particle analysis more difficult. Upon addition of TCD, the colloidal stability significantly improves: nanoparticles appear more isolated and homogeneously distributed. Nonetheless, a trade-off arises between colloidal stability and particle density. As shown in Figure 10, increasing the TCD concentration results in a lower number of nanoparticles per unit area.

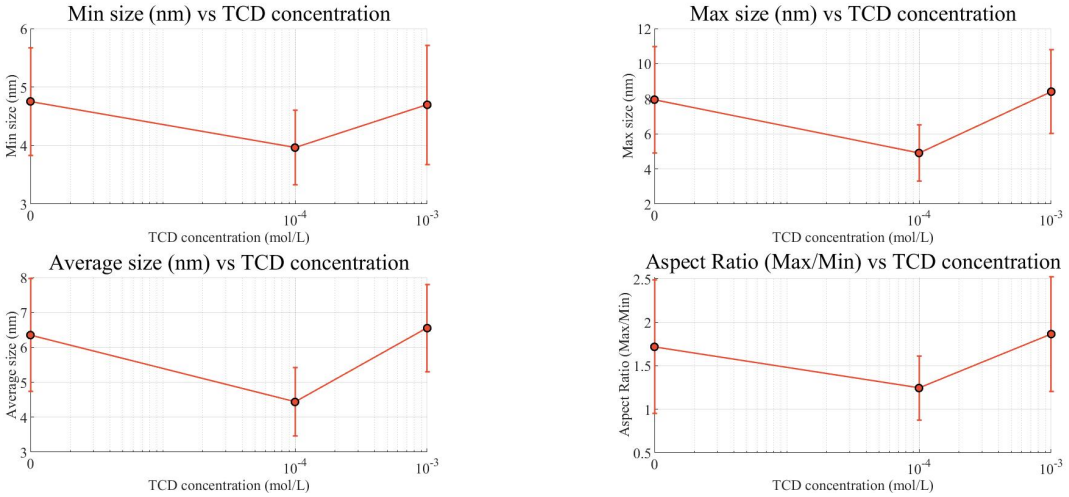

Figure 11: Morphological parameters of nanoparticles synthesized at different TCD concentrations. For visualization on the log scale, the pure water condition was placed at 10^{-6} M. All experiments were performed at 3.07 J/cm^2 for 30 minutes, with 5 Hz repetition rate.

Figure 11 reports the measured size, shape, and aspect ratio of nanoparticles synthesized at varying TCD concentration. The measured parameters remain relatively stable across the tested concentrations, indicating that citrate primarily influences colloidal stability rather than particle growth or morphology.

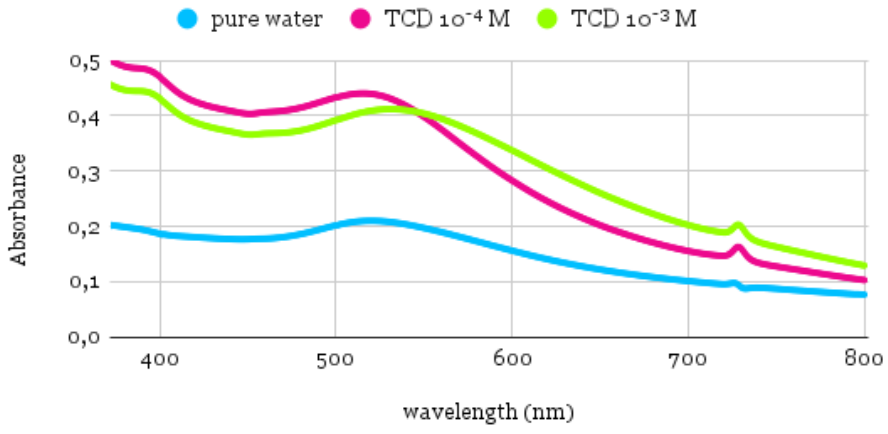

Figure 12: UV-Vis absorbance spectra of samples synthesized at different TCD concentrations. All experiments were performed at 3.07 J/cm^2 for 30 minutes, with 5 Hz repetition rate.

The UV-Vis spectra in Figure 12 further support this interpretation. Both 10^{-4} M and 10^{-3} M TCD concentrations lead to a clear increase in absorbance compared to the sample synthesized in pure water, particularly around the plasmon resonance region near 520 nm. The higher absorbance suggests a greater number of well-dispersed nanoparticles in solution, in contrast to the pure water case, where strong aggregation likely reduces the optical response due to a lower number of isolated nanoparticles. These results are consistent with previous studies [5, 23], which report that moder-

ate concentrations of stabilizing ligands can improve nanoparticle formation while simultaneously preventing aggregation. It should be noted that the small peak observed around 730 nm is most likely a measurement artifact and will therefore be overlooked in the following.
The observed colors of the colloidal solutions, shown in Figure 13, can be explained by considering both nanoparticle concentration and optical properties. The solution prepared in pure water appears very light purple, which is consistent with low absorbance and significant aggregation. indeed, large aggregates scatter light inefficiently and typically result in pale or washed-out colors. In contrast, the sample containing TCD at 10^{-4} M concentration shows a more intense reddish hue, corresponding to a sharper and more pronounced surface plasmon resonance. This indicates a higher concentration of well-dispersed nanoparticles with relatively uniform size.

Surprisingly, the 10^{-3} M sample appears visually lighter, despite exhibiting the highest absorbance in the UV–Vis spectrum. This apparent contradiction can be explained by a lower overall nanoparticle yield. It is known that increasing the concentration of stabilizing agents such as citrate can inhibit nucleation and growth by overly passivating the target surface [5, 23]. Although the particles formed at 10^{-3} M are well dispersed and contribute efficiently to the optical response, their reduced number results in a paler coloration. This interplay between yield and dispersion helps explain why the most vivid color is observed at the intermediate concentration of 10^{-4} M, where both parameters are close to optimal. As mentioned earlier, for TCD concentrations of 10^{-2} M and 10^{-3} M, no nanoparticles were observed, likely due to this passivation effect.

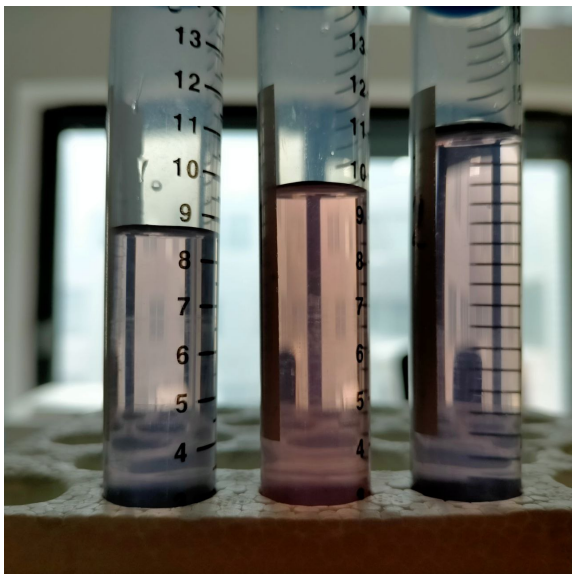

Figure 13: Colloidal gold solutions obtained under the same experimental conditions with different concentrations of ligands. From left to right: pure water, TCD 10^{-4} M, TCD 10^{-3} M.

5.3 Distinguishing the Effect of Ablation and Irradiation in the 10^{-4} M TCD solution

Effect of Ablation Time

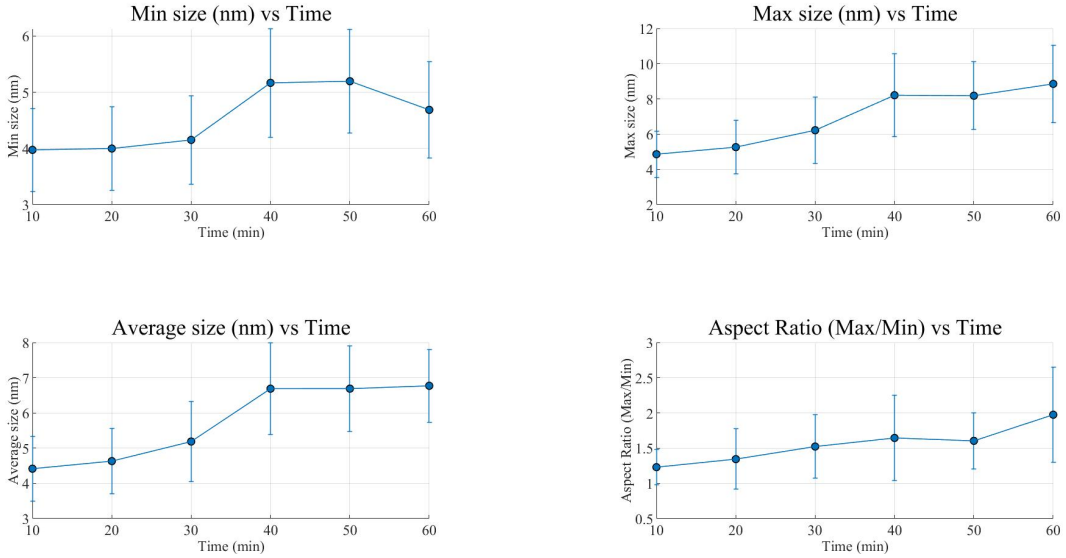

Figure 14: Effect of ablation time on nanoparticle morphology at a ligand concentration of 10^{-4} M TCD. The plots show the evolution of average size, minimum and maximum dimensions, and aspect ratio as a function of irradiation duration. For each experiment, fluence was set at 3.07 J/cm^2 and repetition rate to 5 Hz.

As shown in Figure 14, increasing the ablation time leads to a progressive increase in the average, minimum, and maximum dimensions of the nanoparticles. This trend suggests that prolonged ablation promotes additional growth, likely driven by particle coalescence. Moreover, the aspect ratio also rises with time, suggesting a gradual deviation from spherical geometry toward more anisotropic morphologies, such as ellipsoids or rod-like structures.

The UV–Vis spectra in Figure 15 reflect the morphological evolution associated with increasing ablation time. A gradual redshift of the surface plasmon resonance (SPR) peak is observed, consistent with the formation of larger nanoparticles via coalescence. This redshift is a well-documented phenomenon and results from the enhanced polarizability of the conduction electron cloud in larger particles, which leads to a resonance at longer wavelengths [5, 16, 23].

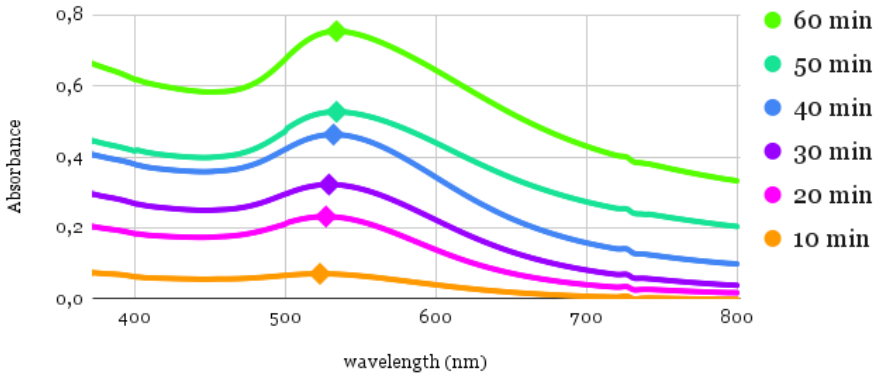

(a) Full spectral range.

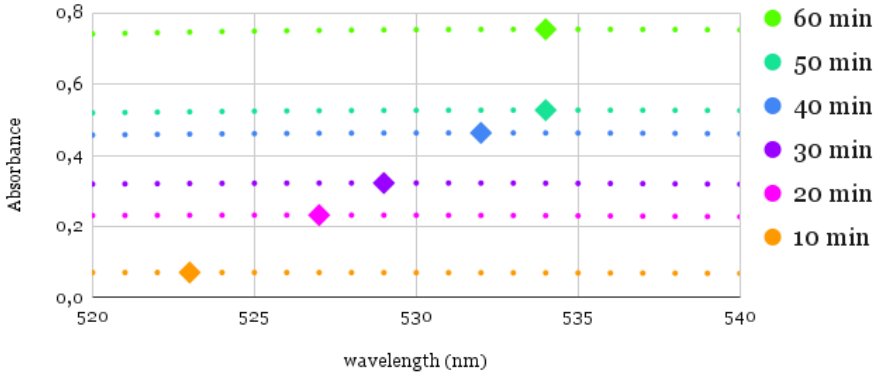

(b) Zoom on the 510–550 nm range. Diamond symbols mark the SPR peak position.

Figure 15: UV-Vis absorbance spectra of nanoparticle colloidal solutions obtained at increasing ablation times (10 to 60 minutes). A global increase in absorbance is observed, accompanied by a redshift of the plasmon resonance peak.

TEM images in Figure 16 illustrate the optical trends observed in the UV–Vis spectra. As ablation time increases, nanoparticles become more densely packed and begin to exhibit irregular or elongated shapes, particularly in the 40 to 60 minute range. This increased aggregation and deviation from spherical morphology are consistent with the redshift and broadening of the SPR peak, confirming the link between extended ablation, particle growth, and optical behavior.

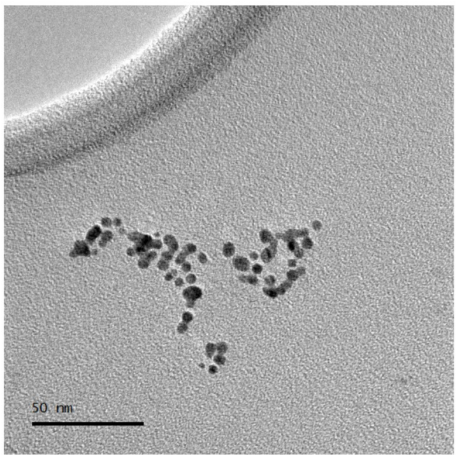

(a) Ablation time: 10 minutes

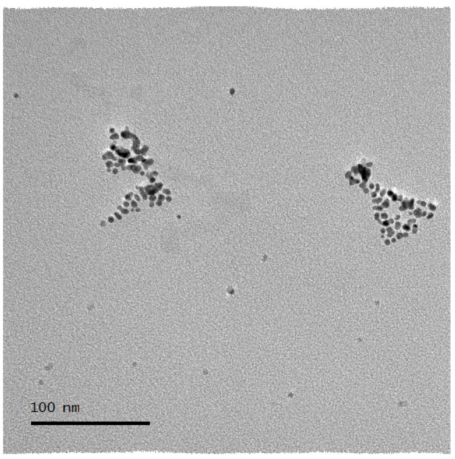

(b) Ablation time: 20 minutes

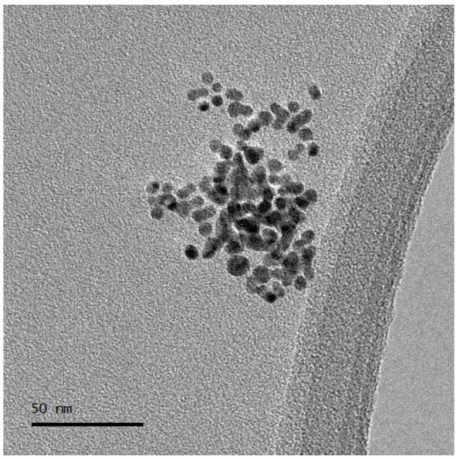

(c) Ablation time: 40 minutes

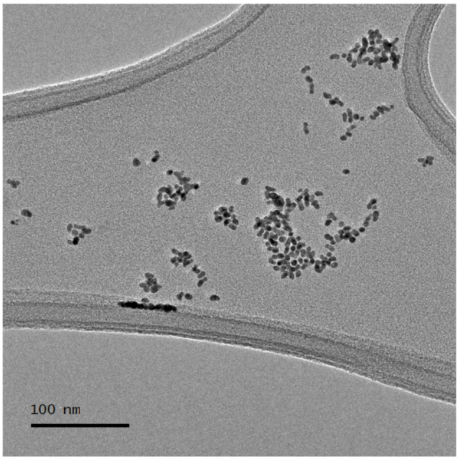

(d) Ablation time: 60 minutes

Figure 16: TEM images of nanoparticles synthesized via laser ablation at increasing durations: a 10 minutes, b 20 minutes, c 40 minutes, and d 60 minutes. Aggregation and shape anisotropy become more evident at longer ablation times.

Effect of Irradiation Time

To evaluate the effect of post-ablation irradiation on preformed colloids, a gold nanoparticle solution synthesized by PLAL in the presence of 10^{-4} M TCD for 60 minutes was subsequently irradiated at a fluence of 2.50 J/cm^2 for 10 and 40 minutes. The resulting UV–Vis absorbance spectra are presented in Figure 17.

Upon irradiation, two main effects are observed: a pronounced decrease in absorbance and a blueshift of the surface plasmon resonance. These changes are consistent with laser-induced fragmentation, a process well documented for colloidal systems exposed to post-synthesis laser treatment in the presence of stabilizing ligands [16, 23]. The reduced absorbance suggests a lower concentration of optically active nanoparticles, possibly due to fragmentation into smaller clusters or sedimentation triggered by localized heating [5, 24]. At the same time, the blueshift presence indicates a decrease in particle size, as smaller gold nanoparticles resonate at shorter wavelengths [21, 23].

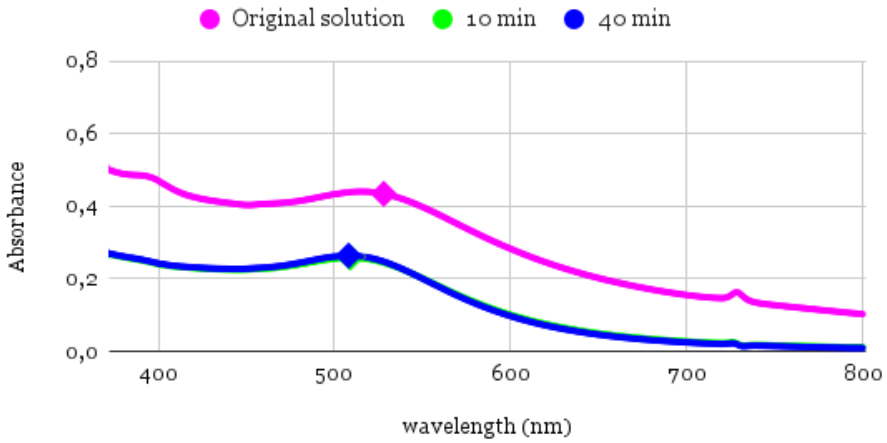

Figure 17: UV–Vis absorbance spectra of gold nanoparticle solutions synthesized by 60 minute ablation and post-irradiated for increasing durations (10 and 40 minutes) at 10^{-4} M TCD concentration. For irradiation, fluence was set at 2.50 J/cm^2 and repetition rate to 5 Hz.

TEM analysis supports these observations, as shown in Figure 18, revealing a clear decrease in both average size and aspect ratio with increasing irradiation time. This indicates that irradiation primarily induces fragmentation of larger clusters into smaller, more uniform nanoparticles. The reduction in aspect ratio also suggests a morphological shift toward more spherical shapes, consistent with previous findings on laser-induced reshaping in citrate-stabilized systems [16, 23].

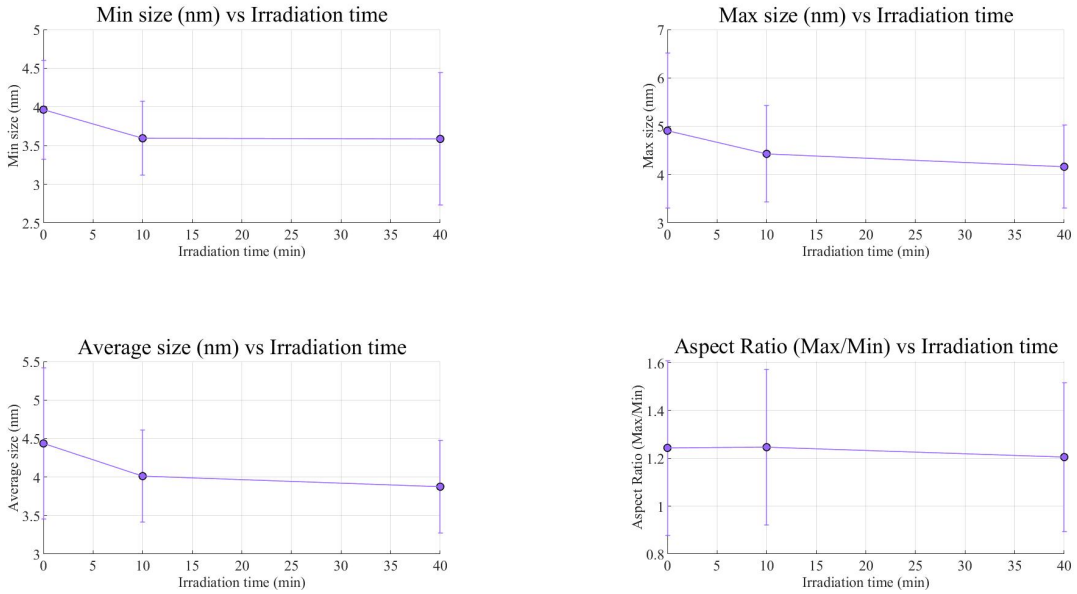

Figure 18: Morphological evolution of nanoparticles under 3.07 J/cm^2 fluence at varying irradiation time. Each subfigure illustrates a distinct size or shape-related parameter, with consistent trends suggesting rapid structural changes within the first 10 minutes.

Altogether, the data show that post-synthesis irradiation in the presence of 10^{-4} M TCD does not trigger further growth or aggregation but instead drives particle refinement through size reduction. Notably, the first 10 minutes of irradiation cause the most significant drop in absorbance and blueshift, underscoring the dual role of laser exposure: it enables size tuning but can reduce colloidal optical activity if applied excessively.

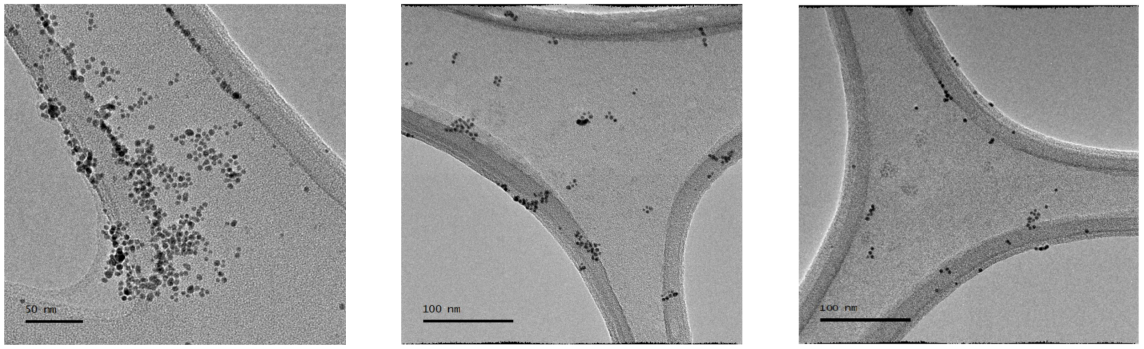

(a) Original solution (b) Irradiation time: 10 minutes (c) Irradiation time: 40 minutes

Figure 19: TEM images of gold nanoparticles obtained after 0, 10, and 40 minutes of post-ablation irradiation at a fluence of 2.50 J/cm^2 and a repetition rate of 5 Hz.

5.4 Distinguishing the Effect of Ablation and Irradiation in the 10^{-3} M TCD solution

Effect of Ablation Time

To properly distinguish the effects of ablation and irradiation, it is important to recognize that during every ablation experiment, the liquid surrounding the target is also irradiated by the laser. As a result, two competing processes occur simultaneously: the growth by coalescence of nanoparticles into larger structures and the fragmentation of larger aggregates into smaller particles. The relative dominance of these mechanisms depends strongly on the ligand concentration and resulting colloidal environment.

At lower TCD concentrations, coalescence and growth are favored, leading to an increase in particle size with longer ablation times. In contrast, at 10^{-3} M, the higher ligand concentration results in a significantly lower nanoparticle density, which suppresses coalescence. Under these conditions, fragmentation becomes the dominant process. This shift in behavior is evident in the 10^{-3} M TCD solution, where increased ligand coverage not only stabilizes the particles against aggregation but also prevents significant coalescence. Although longer ablation durations still increase the number of particles generated, the colloid remains well-dispersed and free from large aggregates.

The UV–Vis spectra in Figure 20 support this interpretation. A steady increase in absorbance is observed with time, yet no redshift of the plasmonic peak is detected. Instead, a slight blueshift occurs, indicating a decrease in average particle size. This observation indicates that the laser-induced fragmentation of nanoparticles in solution is the dominant mechanism rather than coalescence.

TEM analysis (Figure 21) further confirms this trend. With increasing ablation time, nanoparticles become progressively smaller, without any sign of significant aggregation. In contrast to the 10^{-4} M case, where coalescence dominated at long durations, here the colloid exhibits enhanced morphological stability. The higher ligand concentration effectively suppresses aggregation and facilitates a gradual refinement of nanoparticles dimensions over time.

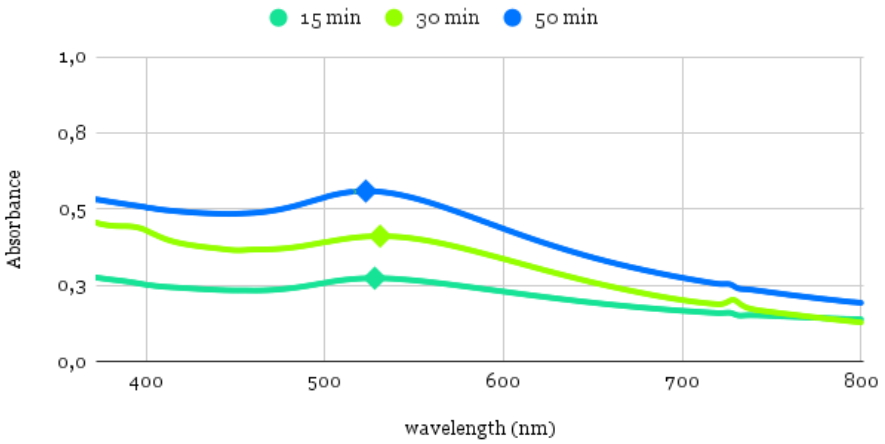

Figure 20: UV–Vis spectra of Au nanoparticles at 10^{-3} M ligand concentration with increasing ablation time (15, 30, and 50 min). A consistent increase in absorbance intensity is observed. For all samples, the ablation fluence was kept constant at 3.07 J/cm^2, with a 5 hz repetition rate.

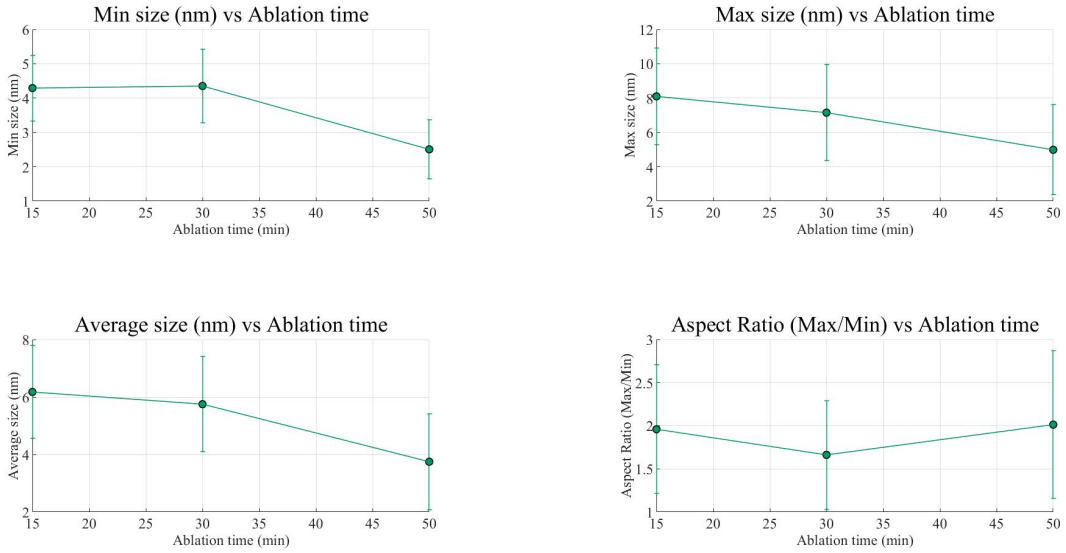

Figure 21: Morphological evolution of nanoparticles under 3.07 J/cm^2 fluence and 5 Hz repetition rate at different ablation times.

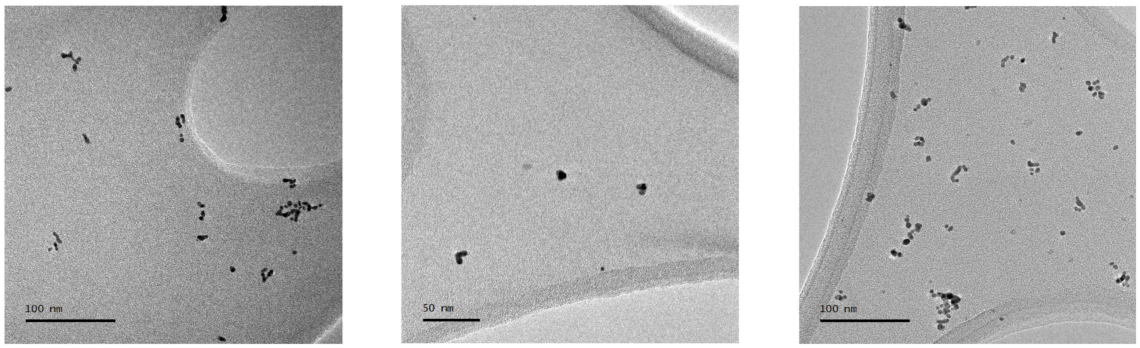

(a) Ablation time: 15 minutes (b) Ablation time: 30 minutes (c) Ablation time: 50 minutes

Figure 22: TEM images of nanoparticles obtained after 15, 30, and 50 minutes of ablation at 3.07 J/cm^2, with a 5 Hz repetition rate.

Effect of Irradiation Time

Consistent with the previously discussed ablation behavior, post-synthesis irradiation of nanoparticles in a 10^{-3} M TCD solution also results in a clear and systematic decrease in nanoparticle dimensions, further confirming the dominance of fragmentation mechanisms. As shown in Figure 23, all morphological parameters decrease progressively with irradiation time. Notably, the most significant changes occur within the first 10 minutes of laser exposure, suggesting that structural transformations are most effective during the early stages of irradiation.

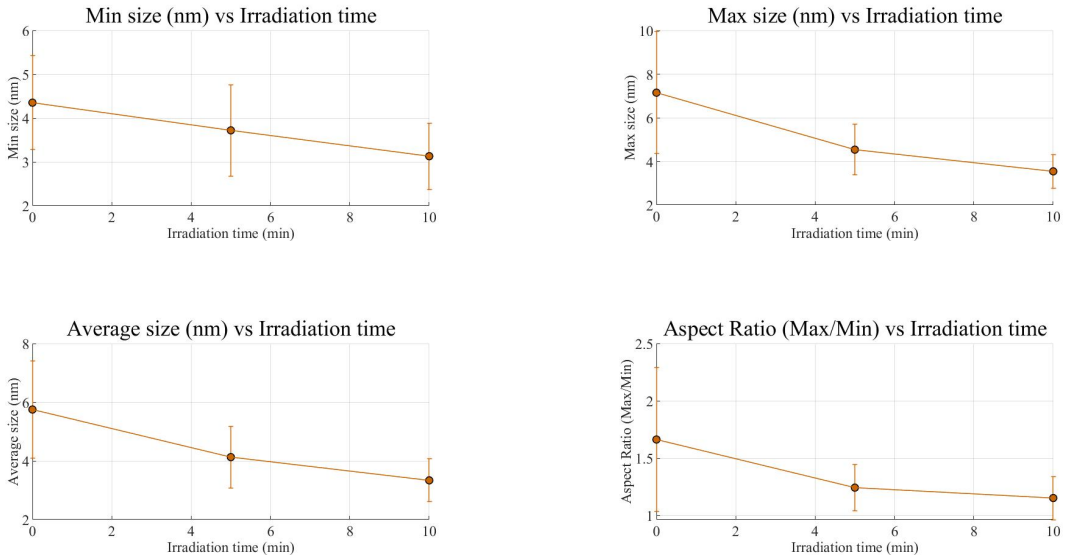

Figure 23: Morphological evolution of nanoparticles under 2.5 J/cm^2 fluence at varying irradiation times.

These morphological changes are supported by the optical response shown in the UV–Vis spectra (Figure 24). A clear blueshift of the plasmon resonance peak is observed with increasing irradiation time, along with a noticeable reduction in absorbance intensity. This behavior confirms the ongoing fragmentation of larger clusters into smaller, less optically active particles.

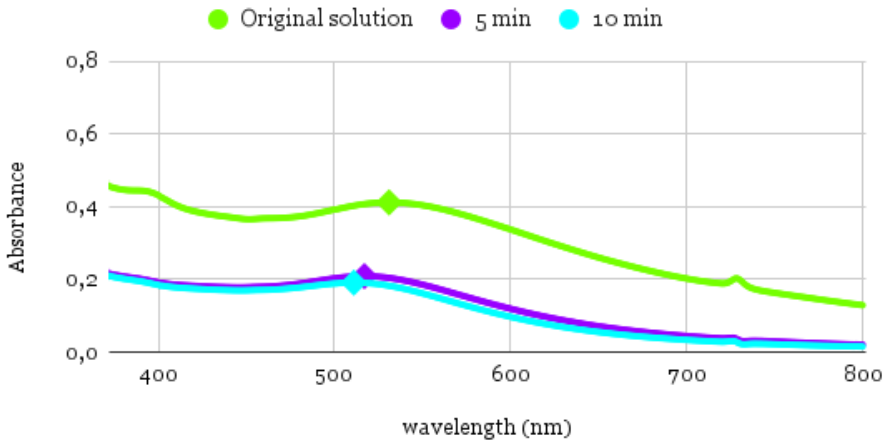

Figure 24: UV–Vis spectra of Au nanoparticles at 10^{-3} M ligand concentration with increasing irradiation time (5 and 10 min). A consistent blueshift and reduction in absorbance intensity are observed. The fluence and repetition rate were kept constant at 3.07 J/cm^2 and 5 Hz respectively.

TEM images in Figure 25 visually confirm this trend. With increasing irradiation time, the nanoparticles appear smaller and more monodisperse. No significant aggregation or morphological irregularities are observed, further supporting the conclusion that progressive size reduction occurs over time.

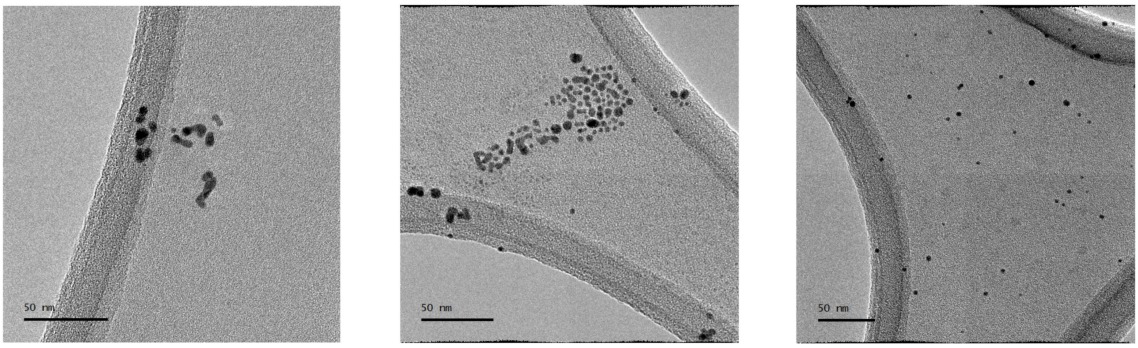

(a) Original solution (b) Irradiation time: 5 minutes (c) Irradiation time: 10 minutes

Figure 25: TEM images of gold nanoparticles obtained after 0, 5, and 10 minutes of post-ablation irradiation at a fluence of 2.50 J/cm^2 and a repetition rate of 5 Hz.

The colloidal solution color also visibly changes with increasing irradiation time, as shown in Figure 26. The color shifts toward lighter shades of purple, consistent with the observed drop in absorbance and particle concentration.

(a) Original solution (b) Irradiation time: 5 minutes (c) Irradiation time: 10 minutes

Figure 26: Evolution of colloidal solution color with irradiation time at 10^{-3} M TCD. The solution becomes visibly lighter, consistent with the decrease in absorbance.

5.5 Alternative Perspective: Using Precursors

As an alternative to the standard pulsed laser ablation in liquid method, a precursor-assisted synthesis approach was explored. In this configuration, no metallic target was employed. Instead, a dilute aqueous solution of tetrachloroauric acid ($HAuCl_4 \cdot 3H_2O$) served as the gold source. The goal was to evaluate whether laser irradiation of a dissolved gold salt could yield nanoparticles with more uniform morphology, improved sphericity, or enhanced colloidal stability.

All experiments were conducted using the same laser and optical setup described in the previous irradiation section. A KrF excimer laser ($\lambda = 248$ nm, nanosecond pulses) was used at a fluence of 2.5 J/cm^2, with pulse energy of 100 mJ, a repetition rate of 5 Hz, and a spot size of approximately 0.03 cm^2. The beam was vertically focused into a 5 mL beaker containing the precursor solution. This small volume was sufficient to ensure strong interaction with the beam while minimizing dilution of reaction products. The evolution of the main morphological parameters is shown in Figure 27.

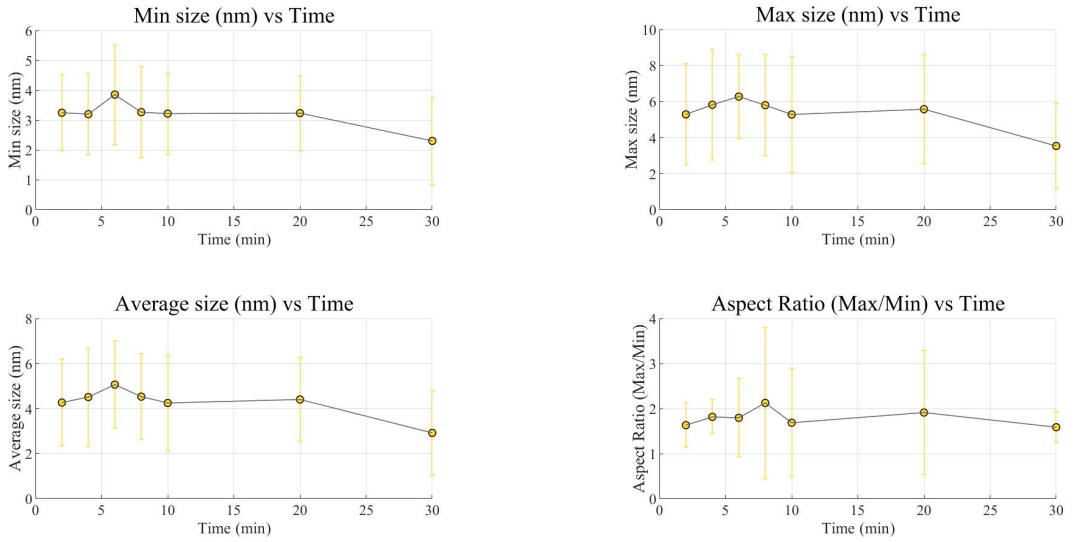

Figure 27: Morphological features of nanoparticles produced from precursor solutions as a function of irradiation time.

In contrast to the trends observed with conventional ablation, the size of nanoparticles synthesized from precursor solutions remained remarkably stable throughout the entire irradiation range, with only minor fluctuations in minimum, maximum, and average dimensions. Interestingly, the average aspect ratio hovered around 1.5, a value generally lower than that observed in all other ablation-based experiments. This result suggests that precursor-assisted photoreduction promotes isotropic nucleation and growth, effectively avoiding the anisotropic effects and shape irregularities typically introduced by high-energy ablation [9].

A direct comparison between these two methods is shown in Figure 28, comparing TEM images of nanoparticles produced via PLAL and precursor-based synthesis under similar irradiation conditions. The difference is evident: while ablation yields particles with more irregular shapes and broader size distribution, the precursor route consistently produces smoother, more monodisperse gold spheres.

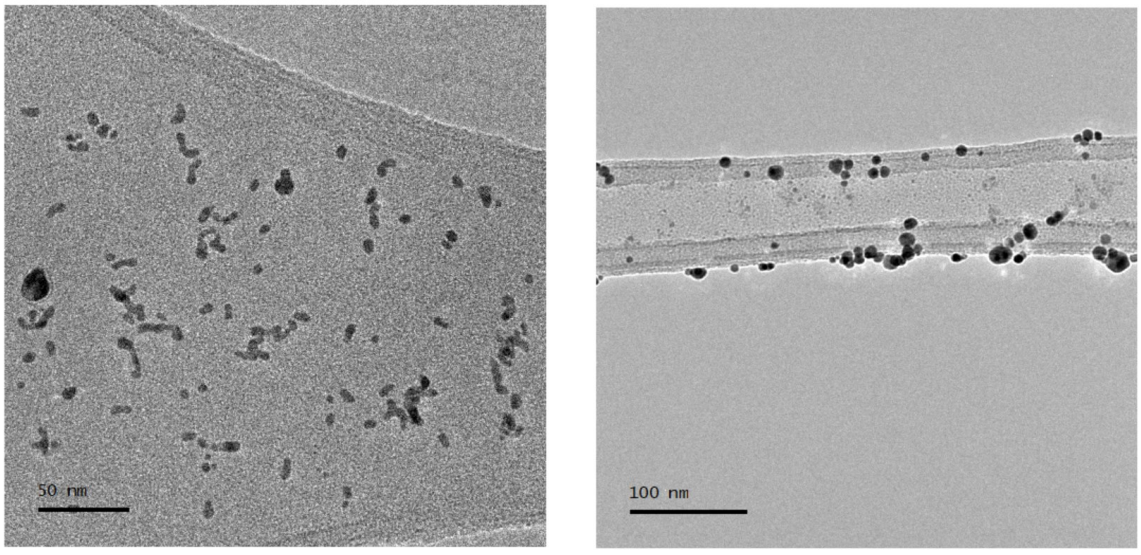

(a) PLAL (15 min, 5 Hz, 3.3 J/cm^2, TCD 10^{-3} M) (b) Precursor solution (20 min, 5 Hz, 2.5 J/cm^2)

Figure 28: TEM images of gold nanoparticles synthesized via (a) PLAL and (b) precursor photoreduction. The latter yields significantly more spherical and uniform particles.

These findings suggest that precursor-assisted photoreduction is a valid alternative to PLAL when the goal is to obtain spherical and uniform nanoparticles. The method is simple, clean, and easily tunable, making it a promising route for controlled nanoparticle synthesis.

6 Conclusions and Perspectives

General Achievements:

- **Reproducibility:** A complete PLAL setup was successfully designed and built, with careful optical alignment and quantitative calibration of laser fluence. The system ensured consistent and repeatable results across ablation, irradiation, and precursor-based experiments.
- **Parameter isolation:** Each synthesis parameter was varied independently to study its specific effect on nanoparticle formation. This approach enabled a clear understanding of how fluence, ablation time, repetition rate, and ligand concentration influence the morphology, size distribution, and optical behavior of the final product.
- **Synthesis optimization:** Experimental conditions were tuned according to different application-driven targets, such as maximizing nanoparticle yield, enhancing colloidal stability, or improving shape uniformity. The comparison between ablation-based and precursor-based synthesis highlighted how the choice of method can be tailored to specific performance goals.
- **Ligand concentration as a functional parameter:** The effect of trisodium citrate dihydrate (TCD) was investigated in detail. Beyond stabilizing the colloid, its concentration was shown to actively influence synthesis dynamics and the absorbance evolution.
- **Ablation and Irradiation:** Dedicated irradiation experiments without the gold target were conducted to isolate the role of solution irradiation, revealing distinct and measurable differences between ablation-driven and irradiation-driven effects.

Key findings:

1. Stabilization through Ligand Addition The addition of trisodium citrate dihydrate (TCD) has a dual effect on colloidal synthesis. On one hand, it reduces nanoparticle aggregation by stabilizing the surface, but on the other, it also lowers nanoparticle density by limiting nucleation events through surface passivation [5, 23]. As a result, the concentration of TCD must be carefully tuned. The most effective range was found to lie between 10^{-4} and 10^{-3} M, where a balance between colloidal stability and sufficient nanoparticle yield is achieved.

2. Influence of Laser Parameters on Synthesis Among all the variables tested, ablation time exhibited the strongest influence on nanoparticle synthesis. A threshold fluence was required to initiate particle formation; however, increasing the fluence beyond this value did not produce significant changes in size or morphology. Similarly, the repetition rate showed minimal impact on nanoparticle dimensions or shape. Overall, these findings highlight ablation time as the dominant parameter in controlling nanoparticle size, while other factors such as fluence and repetition rate play only a secondary role once the necessary energy threshold is exceeded.

3. Effect of Ablation on Nanoparticle Properties
In all cases, ablation led to a net increase in absorbance, as new nanoparticles are continuously generated from the gold target with each laser pulse. However, the evolution of size and optical behavior is strongly dependent on TCD concentration:

- At 10^{-4} M, longer ablation times resulted in a redshift of the plasmonic peak and an increase in average particle size, indicating coalescence-driven growth.
- At 10^{-3} M, by contrast, fragmentation appears to dominate. While absorbance still increases, no coalescence is observed; instead, a slight blueshift emerges. This may result from secondary irradiation effects: as the laser beam passes through the growing colloid, it fragments preformed nanoparticles in a mechanism analogous to that observed in pure post-synthesis irradiation. This effect becomes evident only when coalescence is effectively suppressed, as in the 10^{-3} M case.

4. Effect of Post-Synthesis Irradiation
Unlike ablation, pure irradiation consistently results in a decrease in absorbance. Since no new nanoparticles are formed, the laser primarily acts by breaking down larger clusters into smaller and more spherical fragments. This process produces a characteristic blueshift of the plasmon resonance peak and a reduction in optical density in both the 10^{-4} M and 10^{-3} M cases. The observed behavior is well supported by the literature as a typical outcome of laser-induced fragmentation, which is largely independent of ligand concentration [5, 16, 23].

5. Precursor-Based Synthesis as an Alternative Approach
Using a gold salt solution ($HAuCl_4$) instead of a solid target proved to be a clean and efficient method for synthesizing spherical nanoparticles. While size distributions remained comparable to those obtained via ablation, the particles consistently showed lower aspect ratios and more regular shapes. This makes precursor-assisted photoreduction a promising alternative when shape uniformity is desired, particularly given its simpler setup and the absence of target erosion or debris generation.

6.1 Future Research Directions

This work provided a detailed and systematic investigation of gold nanoparticle synthesis using pulsed laser ablation in liquid (PLAL), with particular focus on the influence of laser parameters and ligand concentration on particle size and morphology. A key strength of the experimental setup developed here is its versatility: it is not limited to gold, and can be readily adapted to ablate a wide range of solid targets.

A natural extension of this study would be to apply the same methodology to more complex materials, such as high-entropy nanoalloys. These multicomponent systems have gained significant attention due to their tunable properties and potential applications in catalysis, energy storage, and biomedical technologies. Investigating their synthesis via PLAL could provide valuable insights into the interplay between composition, ablation dynamics, and resulting nanoparticle structure. Moreover, the approach could help assess whether the tunability observed in monometallic systems like gold carries over to alloy targets, such as the Cantor alloy.

References

[1] Mohammed A. Al-Azawi, Noriah Bidin, Mohamed Bououdina, Abdelelah Alshanableh, and Ethar Yahya Salih. The effects of liquid environment on ablation efficiency and morphology of gold nanoparticles prepared by laser ablation technique. *Journal of Nano Research*, 37:99–108, 2016.

[2] David Alba-Molina, María T. Martín-Romero, Luis Camacho, and Juan J. Giner-Casares. Ion-mediated aggregation of gold nanoparticles for light-induced heating. *Applied Sciences*, 7(9):916, 2017.

[3] Damien Alloyeau, Christian Ricolleau, Claire Langlois, Yann Le Bouar, and Annick Loiseau. Flash laser annealing for controlling size and shape of magnetic alloy nanoparticles. *Beilstein Journal of Nanotechnology*, 1:55–62, 2010.

[4] Damien Alloyeau, Christian Ricolleau, Claude Mottet, Takuya Oikawa, Claire Langlois, Yann Le Bouar, Nabila Braidy, and Annick Loiseau. Size and shape effects on the order-disorder phase transition in copt nanoparticles. *Nature Materials*, 8:940–946, 2009.

[5] H.A. Alluhaybi, S.K. Ghoshal, W.N. Wan Shamsuri, B.O. Alsobhi, A.A. Salim, and G. Krishnan. Pulsed laser ablation in liquid assisted growth of gold nanoparticles: Evaluation of structural and optical features. *Nano-Structures & Nano-Objects*, 19:100355, 2019.

[6] Davide R. Barbero, Tapas K. Ghosh, Carlos E. Gonzalez Soria, Slimane Obbade, Alexandre Rouet, Kenneth R. Shull, Damien Alloyeau, and Vincent Meunier. The role of kinetics in shaping the structure of high-entropy alloy nanoparticles. *Faraday Discussions*, 2024.

[7] A. De Giacomo, M. Dell'Aglio, R. Gaudiuso, O. De Pascale, M. Satta, C. Casavola, G. Giannuzzi, and A. Ancona. Role of the laser pulse duration and energy in laser ablation synthesis of colloidal gold nanoparticles in water. *Journal of Colloid and Interface Science*, 466:129–137, 2016.

[8] D.S.B. Gomes, L.G. Paterno, A.B.S. Santos, D.P.P. Barbosa, B.M. Holtz, M.R. Souza, R.Q. Moraes-Souza, A.V. Garay, L.R. Andrade, P.P.C. Sartoratto, et al. Uv-accelerated synthesis of gold nanoparticle–pluronic nanocomposites for x-ray computed tomography contrast enhancement. *Polymers*, 15(9):2163, 2023.

[9] Gerardo Palazzo. On the stability of gold nanoparticles synthesized by laser ablation in liquids. *Advances in Colloid and Interface Science*, 275:102076, 2020.

[10] Vladimir N. Popok, Pavel Grigoryev, Frank Frost, Julia Elman, Yogesh K. Mishra, and Wolfgang Kessler. Laser-based fabrication and processing of bimetallic nanoparticles. *Solid State Electronics*, 117:22–27, 2016.

[11] Hélène Prunier, Christian Ricolleau, Jaysen Nelayah, Guillaume Wang, and Damien Alloyeau. Original anisotropic growth mode of copper nanorods by vapor phase deposition. *Crystal Growth & Design*, 14(12):6350–6356, 2014.

[12] Guillaume Prévot, Ngoc Tuan Nguyen, Damien Alloyeau, Christian Ricolleau, and Jaysen Nelayah. Ostwald-driven phase separation in bimetallic nanoparticle assemblies. *ACS Nano*, 10(4):4127–4133, 2016.

[13] David Sebastian Redka, Jan Winter, Christian Gadelmeier, Alexander Djuranovic, Uwe Glatzel, Ján Minár, and Heinz Paul Huber. Control of ultrafast laser ablation efficiency by stress confinement due to strong electron localization in high-entropy alloys. *Applied Surface Science*, 594:153427, 2022.

[14] D. Riabinina, A. De Giacomo, M. Dell'Aglio, R. Gaudiuso, O. De Pascale, G. Valenza, P. Alifano, A. De Stradis, and M. De Giorgi. The effects of liquid environment on ablation efficiency and morphology of gold nanoparticles synthesized by pulsed laser ablation in liquid. *Applied Surface Science*, 258(19):7584–7588, 2012.

[15] D. Riabinina et al. Size control of gold nanoparticles synthesized by laser ablation in liquid: influence of laser parameters and concentration of trisodium citrate. *Thin Solid Films*, 482(1-2):151–155, 2005.

[16] G. Schmidl, G. Jia, A. Gawlik, J. Kreusch, F. Schmidl, J. Dellith, A. Dathe, Z.-H. Lin, J.-S. Huang, and J. Plentz. Fabrication of self-assembled spherical gold particles by pulsed uv laser treatment. *Scientific Reports*, 8:11283, 2018.

[17] Reza Shahbazi, Morteza Ghadimi, and Masoud Salavati-Niasari. Effect of laser ablation parameters on gold nanoparticle synthesis in liquid: Toward better understanding of the underlying mechanism. *Materials Chemistry and Physics*, 235:121738, 2019.

[18] Yasuhiro Shiraishi, Eri Shirakawa, Kazuya Tanaka, Hirokatsu Sakamoto, Satoshi Ichikawa, and Takayuki Hirai. Spiropyran-modified gold nanoparticles: Reversible size control of aggregates by uv and visible light irradiations. *ACS Applied Materials & Interfaces*, 6(10):7554–7562, 2014.

[19] Lasse K. Sørensen, Daniil E. Khrennikov, Valeriy S. Gerasimov, Alexander E. Ershov, Sergey P. Polyutov, Sergey V. Karpov, and Hans Ågren. Nature of the anomalous size dependence of resonance red shifts in ultrafine plasmonic nanoparticles. *The Journal of Physical Chemistry C*, 126(39):16804–16814, 2022.

[20] Muhammad Tahir, Gerhard Leichtfried, Wajdi Trabelsi, Pavlo Zolotavin, Leonid V. Zhigilei, Stephan Barcikowski, and Philipp Wagener. Synthesis of high entropy alloy nanoparticles by pulsed laser ablation in liquids: Influence of medium and target composition. *ChemNanoMat*, 10(6):e202300598, 2024.

[21] Kazuo Tanaka, Kensuke Naka, Eisuke Miyoshi, Asako Narita, and Yoshiki Chujo. Control of interparticle spacing in stable aggregates of gold nanoparticles by light irradiation. *Polymer Journal*, 47(10):747–752, 2015.

[22] Alfio Torrisi, Benedetta Fazio, Mariapompea Cutroneo, Giuseppe Compagnini, Francesco Barreca, Francesco Neri, Elisabetta Barletta, Silvana Romano, and Riccardo Raffaele. Laser ablation synthesis of gold nanoparticles in water and biological solutions. *Applied Surface Science*, 252(13):5139–5144, 2006.

[23] Himanshu Tyagi, Ajay Kushwaha, Anshuman Kumar, and Mohammed Aslam. A facile ph controlled citrate-based reduction method for gold nanoparticle synthesis at room temperature. *Nanoscale Research Letters*, 11:362, 2016.

[24] O. Van Overschelde, P. Lievens, and A. Bogaerts. Dynamics of gold nanoparticles generation by laser ablation in liquids. *Laser Physics*, 23(5):055901, 2013.

[25] Hongbo Zeng, Xi-Wen Du, Haoyang Wang, Xiang Zhang, and Liying Xie. Effects of ambient environment and liquid properties on the size and morphology of gold nanoparticles synthesized by laser ablation in liquid. *Nanomaterials*, 7(9):268, 2017.